AGU PUBLICATIONS

JGR

Journal of Geophysical Research: Space Physics

RESEARCH ARTICLE
10.1002/2017JA024482

Special Section:
Magnetospheric Multiscale (MMS) mission results throughout the first primary mission phase

Key Points:
- Provide the reason why the current density was filamentary current within flux ropes which was found recently by MMS
- Confirm coalescence between two neighboring flux ropes and no interaction between two other neighboring flux ropes
- Present the reason why two neighboring flux ropes were interacting and the other two were not

Correspondence to:
R. Wang and Q. Lu,
rswan@ustc.edu.cn;
qmlu@ustc.edu.cn

Citation:
Wang, R., Lu, Q., Nakamura, R., Baumjohann, W., Russell, C. T., Burch, J. L., …, Gershman, D. (2017). Interaction of magnetic flux ropes via magnetic reconnection observed at the magnetopause. *Journal of Geophysical Research: Space Physics*, *122*, 10,436–10,447. https://doi.org/10.1002/2017JA024482

Received 20 JUN 2017
Accepted 11 SEP 2017
Accepted article online 14 SEP 2017
Published online 28 OCT 2017

Interaction of Magnetic Flux Ropes Via Magnetic Reconnection Observed at the Magnetopause

Rongsheng Wang[1], Quanming Lu[1], Rumi Nakamura[2], Wolfgang Baumjohann[2], C. T. Russell[3], J. L. Burch[4], R. E. Ergun[5], P. A. Lindqvist[6], Shui Wang[1], Barbara Giles[7], and Dan Gershman[7]

[1]CAS Key Laboratory of Geospace Environment, Department of Geophysics and Planetary Science, University of Science and Technology of China, Hefei, China, [2]Space Research Institute, Austrian Academy of Sciences, Graz, Austria, [3]Earth Planetary and Space Sciences, University of California, Los Angeles, CA, USA, [4]Southwest Research Institute, San Antonio, TX, USA, [5]Department of Astrophysical and Planetary Sciences, University of Colorado Boulder, Boulder, CO, USA, [6]School of Electrical Engineering, Royal Institute of Technology, Stockholm, Sweden, [7]NASA, Goddard Space Flight Center, Greenbelt, MD, USA

Abstract Using the high-resolution field and plasma data obtained from the Magnetospheric Multiscale mission at the magnetopause, a series of three flux transfer events was observed one after another inside southward ion flows, without time gap between any two successive flux ropes. Using the plasma measurements, the current densities within the flux ropes were studied in detail. The currents within the first two flux ropes, dubbed Fr1 and Fr2, were composed of a series of well-separated filamentary currents. The thickness of the filamentary currents and the gap between them were sub ion scale, occasionally dropped down to electron scale. In the third flux rope Fr3 which was closest to the expected reconnection X line, the current displayed a singular compact current layer, was ion scale in width and concentrated on its center. Considering the location of the flux ropes relative to the reconnection X line, we suggested that the current density could be a singular structure when the flux rope was just created and then fragmented into a series of filamentary currents as time. By examining the interregions between Fr1 and Fr2, and between Fr2 and Fr3, reconnection was only confirmed to occur between Fr2 and Fr3 and no reconnection signature was found between Fr1 and Fr2. It seems that magnetic field compression resulted from collision of two neighboring flux ropes is one necessary condition for the occurrence of the coalescence.

1. Introduction

Magnetic reconnection was applied by Dungey to establish the first open model of the Earth's magnetosphere under the condition of the southward interplanetary magnetic field (IMF) (Dungey, 1961). Southward IMF, the magnetic field lines with opposite directions in the magnetosphere and the magnetosheath will reconnect at the magnetopause and lead to solar wind mass, momentum, and energy transferred into the magnetosphere. Transient events, exhibiting a bipolar signature in the component of the magnetic field normal to the magnetopause, are very common at the magnetopause and called magnetic flux transfer events (FTEs) (Russell & Elphic, 1978). The FTEs are widely regarded as the result of magnetic reconnection at the magnetopause, but the detailed formation mechanisms remain debatable (Hasegawa et al., 2010; Lee & Fu, 1985; Øieroset et al., 2011; Raeder, 2006; Russell & Elphic, 1978; Scholer, 1988; Southwood et al., 1988). FTE shapes, extension in the dawn-dusk direction, evolution, and inner structure have been extensively studied based on spacecraft measurements and theory (Dunlop et al., 2005; Eastwood et al., 2012; Farrugia et al., 2011; Fear et al., 2008; Hwang et al., 2016; Owen et al., 2001; Pu et al., 2013; Teh et al., 2017; Varsani et al., 2014; Zhang et al., 2012; Zhong et al., 2013). The results indicate that the FTEs can be properly modeled by magnetic flux rope structures.

Numerical simulations suggested that the plasmoid instability is the key for accomplishing fast reconnection (Bhattacharjee et al., 2009; Daughton et al., 2009; Daughton et al., 2011; Loureiro et al., 2007; Samtaney et al., 2009) and particle acceleration (Drake et al., 2006; Fu et al., 2006; Oka et al., 2010; H. Wang, Lu, Huang, et al., 2016a). The plasmoids, also called magnetic flux ropes, are continually produced from macroscale to kinetic scale inside the initial current sheet due to the tearing mode (Daughton et al., 2006; Lu et al., 2013) or Kelvin-Helmholtz (Huang et al., 2015), and the formation and interaction of these flux ropes dominate the reconnection evolution. Indeed, a series of magnetic flux ropes are frequently observed one by one at the

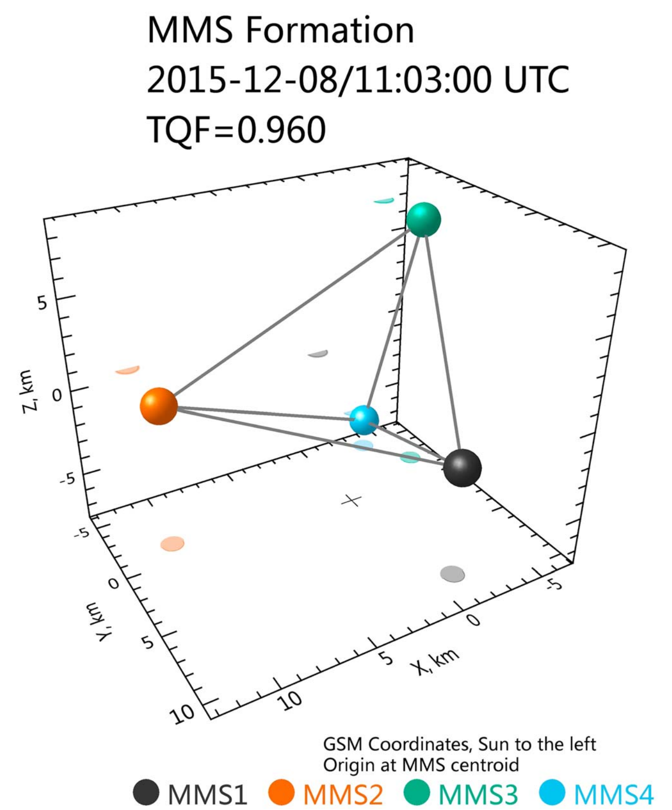

Figure 1. The relative positive of the four MMS satellites at 11:03:24 UT on 8 December 2015. The black red, green, and blue balls represent the four satellites mms1, mms2, mms3, and mms4, respectively.

magnetopause (Dunlop et al., 2005; Eastwood et al., 2016; Fear et al., 2008; Teh et al., 2017). However, their interaction has never been examined at the magnetopause so far. The main reason is obvious that the interaction region between any two neighboring flux ropes is too narrow to be captured by previous spacecraft missions. The novel Magnetospheric Multiscale (MMS) mission launched in 2015 concentrates on electron physics during magnetic reconnection and provides data in unprecedented high resolution (Burch, Moore, et al., 2016), which allows for investigation of the interaction region between two neighboring flux ropes. Based on the MMS measurements at the magnetopause, the ion-scale magnetic flux ropes are identified (Eastwood et al., 2016; Hwang et al., 2016; Teh et al., 2017; Zhao, Russell, et al., 2016), and the current within the flux rope is found to be filamentary (Eastwood et al., 2016). Moreover, the ion frozen in condition is broken while the electrons are still frozen in magnetic field lines inside these ropes (Eastwood et al., 2016; Teh et al., 2017), and some flux ropes are force-free but some are not (Zhao, Russell, et al., 2016). In this paper, we analyze the features of a series of three FTEs within southward ion bulk flows at the magnetopause, present the first evidence for the interaction of the FTEs, and briefly discuss the condition for occurrence of the interaction.

2. Instrumentation and Database

The MMS mission consists of four satellites flying in an elliptical equatorial orbit with geocentric perigee and apogee of 1.2 Earth radii (R_E) and 12 R_E, respectively. The four satellites form a nearly regular tetrahedron (Figure 1) and are equipped with the identical instruments. The first phase of the MMS mission focuses on the dayside magnetopause and the separation is about 10 km. The measurements from several instruments on the MMS spacecraft are used in this paper. The magnetic field is sampled at 128/s (Russell et al., 2016) and the electric field is sampled at 8192/s (Ergun et al., 2016; Lindqvist et al., 2016). The time resolutions for electrons and ions obtained from the fast plasma experiment (Pollock et al., 2016) are 30 ms and 150 ms, respectively.

3. Overview of the Event

At ~11:03 UT on 8 December 2015, MMS was located at [10.5, 1.1, −1.3] R_E in the geocentric solar magnetospheric (GSM) system, with an interspacecraft separation of less than 16 km, as shown in Figure 1 with a color scheme of black for mms1, red for mms2, green for mms3, and blue for mms4. The spacecraft traversed the magnetopause inbound from the magnetosheath to the magnetosphere with an average speed of ~86 km/s. The speed was assessed via the timing method (e.g., Schwartz, 1998) performed to the B_z reversal point at ~1103:05 UT. Figure 2 shows an overview of the magnetopause crossing in the GSM coordinates used throughout this paper.

The spacecraft started to move toward the magnetosphere side from about 1102:50 UT, as shown in Figure 2, and detected the plasma characteristic of the magnetosphere at about 1103:50 UT (not shown). In this process, the spacecraft was located in the low-latitude boundary layer between 1102:50 and 1103:20 UT, since the plasma energy spectrum shows that the energy of the electrons was mainly below 300 eV (Figure 2i) and the ion energy was less than 2 keV (Figure 2j), and the magnetic field component B_z evolved from negative to positive (Figure 2c). In addition, continuous southward ion and electron bulk flows were detected in this interval (red traces in Figures 2f and 2g). Thus, we conclude that a reconnection event was occurring north of the spacecraft. As the spacecraft traversed the low-latitude boundary layer to the magnetosphere side, B_z was substantially enhanced at ~1103:02 UT ($B_z < 0$) and ~1103:12 UT ($B_z > 0$) in Figure 2c, and the duration for each enhancement was about 4 s. Hence, the magnetic field fluxes were compressed on both

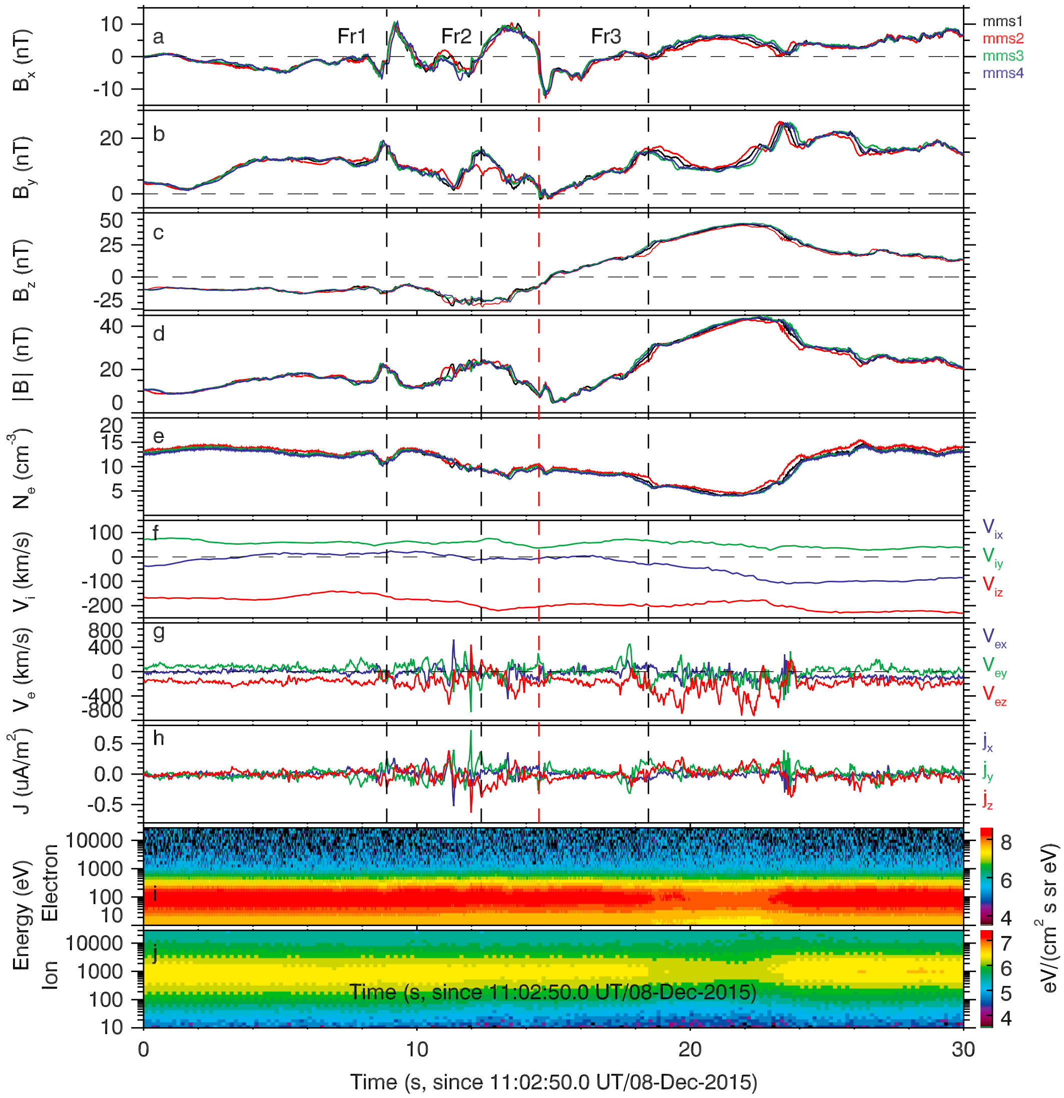

Figure 2. An overview of the flux transfer events. (a–e) Three components and magnitude of magnetic field and electron density at the four satellites with the same color scheme to Figure 1. (f–j) Ion and electron bulk flows, current density $qN(\mathbf{V}_i - \mathbf{V}_e)$, and electron and ion energy spectrum at mms1.

sides of the magnetopause current sheet. The close correlation between the strong flows of electrons (Figure 2g) and the B_z enhancement (Figure 2a) indicates that the strong electron flows can have resulted from the compression. In Figure 2h, the current density calculated from the plasma measurements was intense at both sides of the magnetopause, whereas it is very weak at the point of B_z~0 (at ~11:03:05 UT). It appears that the current sheet was bifurcated at that time.

During this crossing, a series of three magnetic flux ropes were detected in turn. Each of these flux ropes was characterized by a bipolar B_x (Figure 2a) with a significant peak of B_y (Figure 2b) at its center marked by the black vertical dashed line. The total magnetic field intensity was enhanced also at their centers (Figure 2d). The flux ropes are named Fr1–Fr3 according to the detected time (Figure 2a). The axial orientation of these flux ropes are determined by the minimum variance analysis of magnetic field (Sonnerup & Cahill, 1968; Xiao et al., 2004), referred to the principal axis analysis approach (Sibeck et al., 1984; Zong et al., 1997). The results are displayed in Table 1. The ratio of intermediate to minimum eigenvalues is no less than 13 for all events. The intermediate direction was mainly along the y direction in the GSM coordinates. A clear peak of B_y was always observed at the center of each flux rope. Thus, the axial orientations of the flux ropes were primarily along the y direction.

Table 1
Results of Minimum Variance Analysis Applied to the Magnetic Field Data at mms1

Event	Time	Eigenvalue	Eigenvector
Fr1	1102:58–1103:00 UT	0.17	(0.046, 0.563, 0.825)
		5.267	(0.498, 0.703, −0.507)
		35.856	(0.866, −0.434, 0.249)
Fr2	1103:01.5–1103:03.5 UT	1.031	(−0.197, 0.078, 0.977)
		13.854	(0.222, 0.975, −0.032)
		29.14	(0.955, −0.211, 0.209)
Fr3	1103:06.5–1103:10.5 UT	0.418	(0.912, 0.333, −0.241)
		7.066	(−0.359, 0.930, −0.076)
		72.186	(0.199, 0.156, 0.968)

The durations of the three flux ropes based on the peak-to-peak values of B_x were 0.57 s, 1.5 s, and 6.7 s, respectively. Using the four-spacecraft timing method applied to the magnetic field at the flux rope center (the points of $B_x = 0$ for the Fr1 and the B_y peaks for the other two flux ropes), the speed and the propagation direction of the three flux ropes were obtained to be 167 km/s along $\mathbf{n}_1$ = (0.12, −0.30, −0.95) for Fr1, 91 km/s along $\mathbf{n}_2$ = (−0.53, 0.51, 0.68) for Fr2, and 79 km/s along $\mathbf{n}_3$ = (0.93, 0.25, −0.29) for Fr3. Thus, the cross-section diameters of the three flux ropes were 91 km (~1.3 d_i), 118 km (~1.6 d_i), and 609 km (~8.6 d_i), respectively, where the ion inertial length d_i was about 72 km based on the average density (N = 10 cm^{-3}) in the boundary layer. The flux content can be roughly estimated by $\phi = \pi r^2 B$ to be ~200 Wb for the first two flux ropes (Fr1 and Fr2) and to be ~5.0 kWb for the last flux rope (Fr3), if we assume that the flux rope was a cylindrical magnetic field structure. The flux content was underestimated since the spacecraft did not encounter the center of the flux rope ($|B_z|$ ~ 10 nT), that is, the large-impact parameter (Slavin, Lepping, Gjerloev, Fairfield, et al., 2003).

4. Spatial and Temporal Evolution of the Filamentary Currents Within the Flux Ropes

The current density can be directly calculated from the plasma measurements at 30 ms cadence (Burch, Torbert, et al., 2016; Eastwood et al., 2016). Figure 3 shows the current density calculated by the equation $\mathbf{J} = qN(\mathbf{V}_i - \mathbf{V}_e)$, where q is the elementary charge, N is the plasma density, and $\mathbf{V}_i$ and $\mathbf{V}_e$ are the ion and electron bulk flow velocities. The three columns correspond to the three flux ropes. In each column, B_x, the ratio of the perpendicular and parallel current magnitudes $|j_\perp|/j_{//}$; the electric field E_x, $-(\mathbf{V}_i \times \mathbf{B})_x$ and $-(\mathbf{V}_e \times \mathbf{B})_x$; and the current density vectors at the four spacecraft are displayed from top to bottom. The current density vector at the four satellites for Fr1 is shown in Figures 3d–3g. The blue, yellow, and green traces denote the current density components j_x, j_y, and j_z, respectively. The current density is enhanced within Fr1 and the intensities of the three components were comparable. Remarkably, there does not exist a singular current layer inside the Fr1 as observed previously by Cluster (Slavin, Lepping, Gjerloev, Goldstein, et al., 2003; Wang, Lu, Huang, et al., 2016a). In contrast, there were at least two filamentary currents inside Fr1, corresponding to the two j_y peaks at ~1102:58.8 UT and 1102:59.0 UT. The durations for the two filamentary currents were ~100 ms and ~300 ms, and the gap between them was 100 ms. Given the speed of flux rope Fr1, the width of the filamentary currents was 16 km (~0.2 d_i or 9 d_e, where $d_e \approx$ 1.7 km is electron inertial length) and 48 km (~0.7 d_i), respectively. So the thickness of the filamentary current was sub ion scale, even down to electron scale. The widths of the filamentary current and the gap between them were comparable. Although the two filamentary currents j_y were detected by all four satellites, the intensity of the first filamentary current at mms2 was weaker than those observed at other three satellites. The reason can be that mms2, which was 11 km earthward away from other three satellites (Figure 1), traversed the edge of the filamentary currents.

The mms4 was southmost (Figure 1) and therefore passed the Fr1 last, which is seen in Figure 3a, where mms4 observed the bipolar B_x after other three satellites. The probe mms4 was between mms1 and mms3 in the x direction, and the distance between mms4 and mms3 or mms1 was less than 3 km in this direction. Moreover, mms4 was very close to mms3 in the y direction (~3 km) and was widely separated in the z direction from mms3 (~13 km). The separation between mms3 and mm4 in the x and y directions (~3 km) was much less than the thickness of the second filamentary current (~48 km). Considering that the filamentary current was moving mainly southward, therefore the difference of the current density j_y at mms3 and mms4 could be due to evolution of the filamentary current. Comparing the second filamentary currents at mms3 and at mms4, mms3, which crossed the current at first, observed only one peak (Figure 3f) while mms4, which crossed the current at last, observed two small j_y peaks at 1102:59.0 UT (Figure 3g). So it seems that the second filamentary current was fragmenting into two smaller filamentary currents at that time.

A series of well-separated filamentary currents were detected as well in Fr2 (Figures 3k–3n). There were more filamentary currents inside Fr2 than Fr1. Comparing the current density j_y at the four satellites, a very intense filamentary current (up to 1.0 μA/m^2) was observed by mms3, mms1, and mms4 in turn at ~1103:02 UT, but

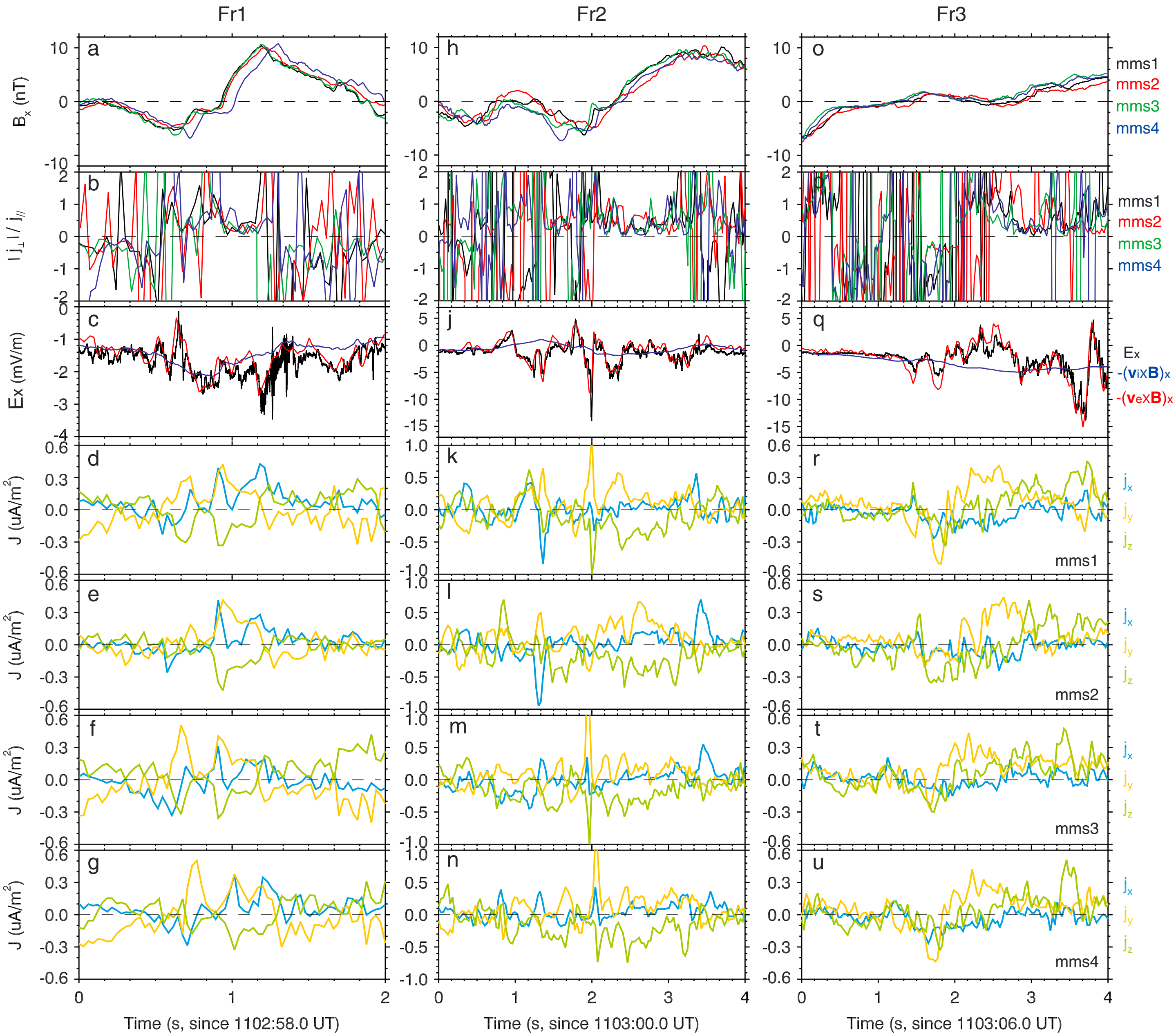

Figure 3. (a–g) B_x and the ratio of $|j_\perp|/j_{//}$ from the four satellites; the electric field E_x, $-(\mathbf{V}_i \times \mathbf{B})_x$, and $-(\mathbf{V}_e \times \mathbf{B})_x$; and three components of the current density from the four satellites for the flux rope Fr1. (h–u) The data in the same format for the flux ropes Fr2 and Fr3.

mms2 did not detect any signature of such intense current (Figure 3l). The duration for this intense filamentary current was ~80 ms, and the corresponding width was ~6 km≈4 d_e. So mms2, 11 km earthward away from other satellites in the x direction (Figure 1), did not encounter this filamentary current in electron scale. There were also sub ion-scale currents inside Fr2, for example, the currents at ~1103:02.2 observed by mms1 and mms2. Based on the analysis above on Fr1 and Fr2, a few filamentary currents were observed inside the flux ropes; the filamentary currents were separated, and their thicknesses were sub ion scale, even down to electron scale sometimes. The width of the gap between the filamentary currents was comparable to the scale of the filamentary current itself. In contrast, the appearance of the current density within the Fr3 was different. Inside Fr3, the current density j_y displayed a singular current layer for 1 s (~1103:08–~1103:09 UT) with a few further localized enhancements (the

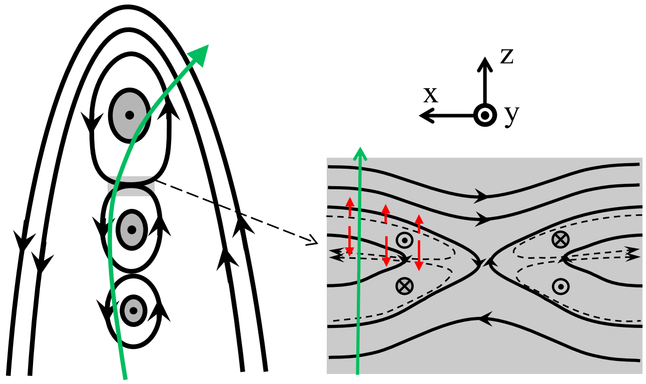

Figure 4. A schematic illustration for the flux ropes and the reconnection of the coalescence. (left column) The three flux ropes detected in the south of a reconnection X line. The green curve with an arrow means the MMS trajectory relative to the structure. (right column) The schematic illustration for the ion diffusion region of asymmetric reconnection. The dashed lines denote the Hall electron current system. The red arrows pointing to the south represent the Hall electric field, while the arrows directed to the north mean Larmor electric field.

small peaks in Figures 3r–3u). The thickness of this singular current layer was estimated to be 79 km ~ 1 d_i. Ahead of this singular current layer, a negative j_y (down to -0.5 μA/m^2) at 1103:07.7 UT was observed by all four satellites. It is unclear how a negative j_y was produced within a flux rope at the magnetopause.

Figures 3c, 3j, and 3q show the measured electric field E_x in black, $-(\mathbf{V}_i \times \mathbf{B})_x$ in blue, and $-(\mathbf{V}_e \times \mathbf{B})_x$ in red from mms1. E_x and $-(\mathbf{V}_e \times \mathbf{B})_x$ matched pretty well while $-(\mathbf{V}_i \times \mathbf{B})_x$ was deviated from E_x. The same results can be obtained from other three satellites. Therefore, the electrons were still frozen in the magnetic field lines, whereas ions were not within all three flux ropes. This result is consistent with the previous observations by MMS (Eastwood et al., 2016; Teh et al., 2017). Figures 3b, 3i, and 3p display the ratio of $|j_\perp|/j_{//}$ at the four satellites. The current ratio changed largely and randomly but kept nearly constant (1102:58.90–1102:59.15 UT for Fr1 and 1103:02.16–1103:03.0 UT for Fr2) around the center of the ropes Fr1 and Fr2. It indicates that the magnetic field tended to be force-free around the central regions while it was nonforce free in most other regions (e.g., the boundary of the flux ropes) at the Fr1 and Fr2. The situation was distinct at the Fr3. Within the Fr3, the ratio always changed substantially and kept a low values during 1103:08.5–1103:09.2 UT (Figure 3p). Even in such short period, however, the ratio at the mms2 was still varying significantly. So the magnetic field was not force-free at the Fr3.

5. Interaction of Two Neighboring Flux Ropes via Magnetic Reconnection

The three flux ropes were observed one after another in the southern ion bulk flows, as illustrated in Figure 4 (the left column). There was almost no time gap between them, especially between Fr2 and Fr3 (Figure 2a). Thus, we tried to figure out whether these flux ropes were interacting. As for the Fr1 and Fr2, the leading part of the Fr2 met the trailing part of the Fr1 at about 11:03:00 UT. However, the induced current layer, which was thought to be one necessary condition for occurrence of the coalescence, was not observed between Fr1 and Fr2 at the moment. Thus, there was not any signature associated with coalescence or reconnection found. Approximately 1.5 s later, a narrow electron jet v_{ex} up to 400 km/s was indeed observed (Figure 2g). However, this electron jet was detected within the Fr2 and was only encountered by mms1 and mms2. The similar electron jet can be found also at 1103:03 UT and at 1103:09 UT. So the narrow electron jets could be due to the compression of the localized magnetic field B_z as mentioned above.

The trailing part of the flux rope Fr2 was closely followed by the leading part of the Fr3. Hence, B_x changed from positive to negative at 1103:04.5 UT (the red vertical dashed line in Figure 2) in the southern ion flow. In order to confirm whether the reconnection was occurring there, the interregion between them was enlarged in Figure 5. A dawn-ward electric current layer (j_y) was observed just at the reversal point of B_x (Figure 5f). The solid and the dashed curves in Figure 5f denote the total and electron current densities, respectively. So the electric current j_y was mainly carried by the electrons and was formed by the electron bulk flow in the y direction (Figure 5e). The direction of this current was contrary to the normal current at the magnetopause and it pointed to the dawnside. Figures 5a–5c shows the three components of the magnetic field at the four satellites. B_x gradually decreased from 6 nT to 0 nT at about 1103:04.5 UT, corresponding to the trailing part of Fr2, and then continued to fall to -12 nT at about 1103:04.7 UT (the leading part of Fr3). Obviously, the magnetic field component B_x was significantly asymmetric at both sides of the current layer. The maximum value of B_x at the left side in Figure 5 (or the bottom in the right column of Figure 4) was 5 nT, while the value was -12 nT at the other side. Considering that the four satellites crossed this current layer one by one, we estimated its normal direction and the propagation velocity by the timing method. The timing method was performed to the B_x reversal points at the four satellites. The result indicates that the current layer was propagating at a speed of 167.4 km/s along [-0.115, 0.303, 0.946] GSM relative to the spacecraft. Thus, the current layer was primarily lying in the $x-y$ plane and its thickness was estimated

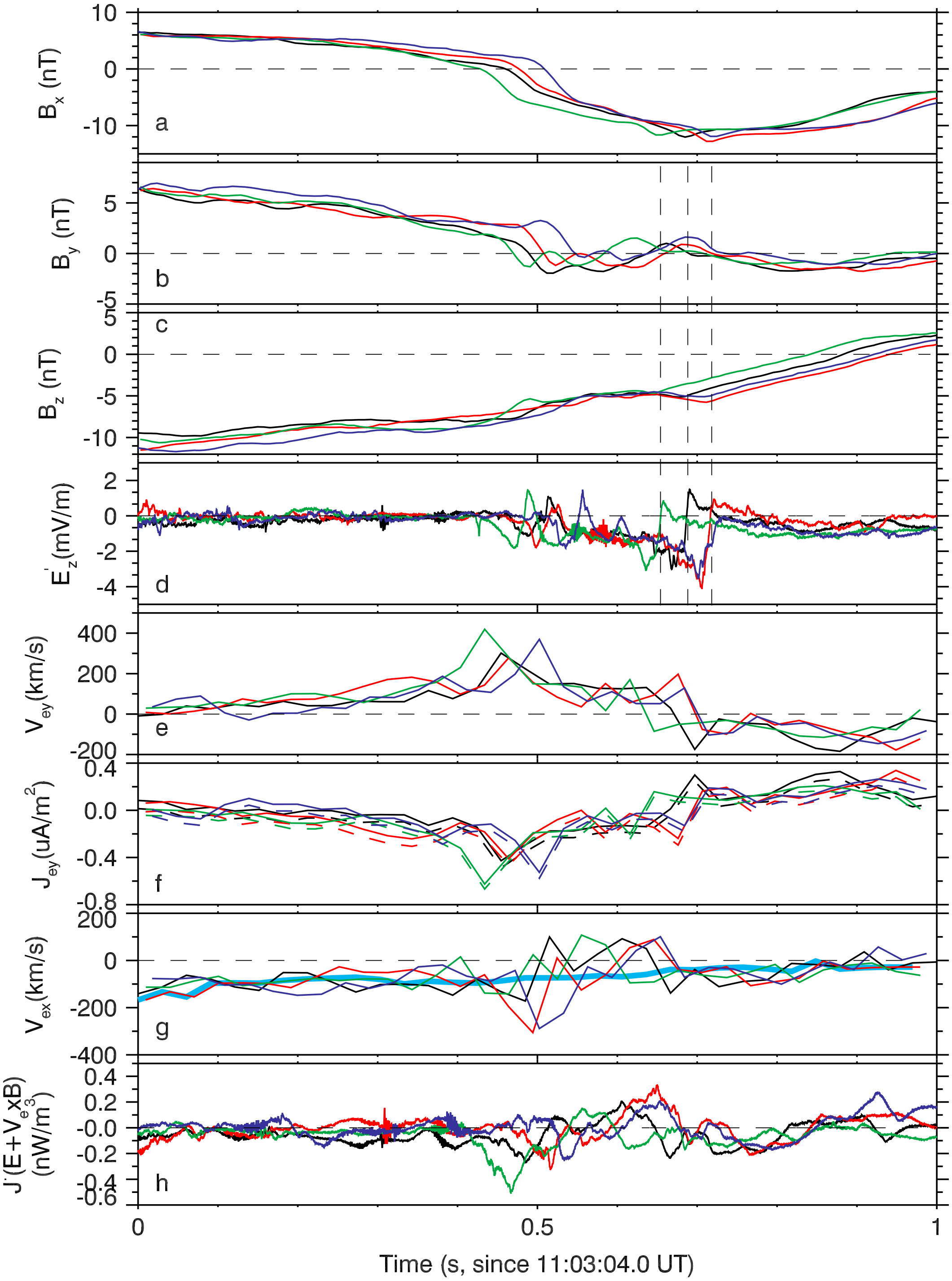

Figure 5. The magnetic field components (a) B_x, (b) B_y, (c) B_z, (d) $E_z' = (\mathbf{E} + \mathbf{V}_{\mathrm{X\ line}} \times \mathbf{B})_z$, (e) the electron velocity in the *y* component V_{ey}, and (f) the electric current density in the *y* direction. The solid and dashed curves denote the total current density and the electron current density, respectively. (g) The electron velocity in the *x* direction. The thick pale blue line represents the average speed at all four satellites. (h) $\mathbf{J} \cdot (\mathbf{E} + \mathbf{V}_e \times \mathbf{B})$.

to be 63 km ~ 0.9 d_i. Comparing the B_x magnitudes in the leading and trailing part of the Fr3 in Figure 2a, we can find that the B_x intensity in the leading part of the Fr3 was significantly larger than that in the trailing part of the Fr3. It can be caused by the collision between Fr2 and Fr3. Therefore, the current layer between them was induced in the interaction region.

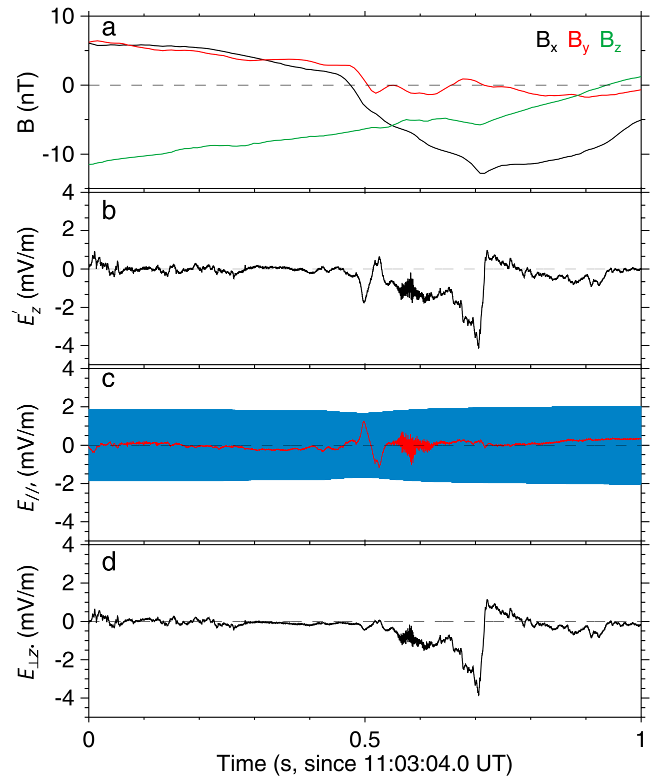

Figure 6. The measurements of electric field at mms2 are presented. (a) Three components of magnetic field. (b–d) $E_z' = (\mathbf{E} + \mathbf{V}_{X\ \text{line}} \times \mathbf{B})_z$, $E_{//}$, and $E_{\perp z}$.

The magnetic field component B_y was gradually decreasing (Figure 5b) as the spacecraft approached the center of the current layer. Around the center of the current layer (~1103:04.5 UT), a bipolar B_y signature from negative to positive was observed at all four satellites. Given the MMS trajectory relative the current layer in Figure 4, the bipolar B_y signature is consistent with the expected Hall magnetic field in the reconnection outflow. The duration of the negative B_y part was longer than the positive part, which can be found also in Figure 6a (the red trace). This kind of asymmetric Hall field has been confirmed recently in asymmetric reconnection (Wang et al., 2017). Figure 5d presents the electric field E_z' in the frame of the current layer. E_z' was mainly negative, that is, pointing southward in Figure 4, and changed sign at the northern edge of the Hall magnetic field (marked by the vertical dashed lines). The southward E_z' was consistent with the Hall electric field, and the following northward E_z' was in agreement with the Larmor electric field observed in asymmetric reconnection (Koga et al., 2014; Malakit et al., 2013). Therefore, the Hall magnetic field and Hall electric field were detected while the spacecraft passed through the interaction region between the Fr2 and Fr3. In other words, a reconnection was taking place between them.

In addition to the E_z' sign change at the north edge of the Hall magnetic field, another E_z' perturbation was observed at 1103:04.5 UT near the south edge of the Hall magnetic field (Figure 5d). In order to distinguish the bipolar E_z' signatures at the south and north edges of the Hall magnetic field, we calculated the parallel and perpendicular electric fields shown in Figures 6c and 6d. It is clear that the E_z' perturbation at the south edge (~1103:04.5 UT) mainly came from the parallel electric field, whereas the E_z' perturbation at the north edge (~2204:04.65 UT) came from the perpendicular component. Apparently, the E_z' perturbation at the south edge of the Hall magnetic field region represents electrostatic isolated waves. The electrostatic waves in the separatrix region are frequently observed (e.g., Ergun et al., 2009; Wang et al., 2014). The unipolar parallel electric field, called electric double layer, followed by a series of electron holes was confirmed previously (Wang et al., 2014). Generally, the duration of the double layer is much longer than that of the electron hole (Ergun et al., 2009; Wang et al., 2014). In contrast, a bipolar parallel electric field (duration ~50 ms) followed by a train of high-frequency electron holes was observed in this event. Since the electrostatic waves were observed at the south edge of the Hall magnetic field and accompanied by the inflowing electrons, they can be created by the electron beam instability (Newman et al., 2001). The measurement of the parallel electric field further indicates that the reconnection was occurring between Fr2 and Fr3 (Hesse & Schindler, 1988). On the other hand, the E_z' perturbation at the north edge corresponded to the Hall electric field.

Within the Hall magnetic field region, an electron bulk flow in the +*x* direction, relative to its background flow (the thick pale blue curve in Figure 5g), was observed at ~1103:04.6 UT from all four satellites. This electron bulk flow in the +*x* direction was as large as 160 km/s relative to the background speed, and the local Alfven speed was about 140 km/s ($|\mathbf{B}| \approx 20$ nT and $N_i \approx 10$ cm^{-3}). Thus, this electron flow can be the electron outflow of the coalescence. Furthermore, this electron outflow was bounded by the electron flow in the $-x$ direction at each spacecraft. At ~1103:04.5 UT, the negative electron flow relative to the background flow was observed just at the south edge of the Hall magnetic field, while after ~1103:04.7 UT, another negative electron flow was measured at the north edge of the Hall field. These negative electron flow relative to the background flow corresponded to the inflowing electrons during reconnection. So these electron bulk flows constitute the full Hall electron current system in one side of the reconnection outflow region, as illustrated in Figure 4 (the dashed curves). At the south edge of the Hall field, the speed of the inflowing electrons was comparable to the electron outflows, which could be the reason for the E_z' perturbation observed there. The energy dissipation quantity $\mathbf{J} \cdot (\mathbf{E} + \mathbf{V}_e \times \mathbf{B})$ in the electron frame (Zenitani et al., 2012) is displayed in Figure 5h. The values of $\mathbf{J} \cdot (\mathbf{E} + \mathbf{V}_e \times \mathbf{B})$ were very small (~0.2 nW/m^3), in comparison with the observation near the electron diffusion region (~10 nW/m^3) (Burch, Torbert, et al., 2016; Wang et al., 2017). It means that the mms spacecraft did not observe the inner electron diffusion region of the coalescence.

6. Discussion and Summary

The magnetic flux rope represents a kind of the helical magnetic structure and has been often observed inside the current sheet at the magnetopause (Dunlop et al., 2005; Fear et al., 2008; Russell & Elphic, 1978; Scholer, 1988; Southwood et al., 1988; Teh et al., 2017) and in the magnetotail (Sibeck et al., 1984; Moldwin & Hughes, 1991; Slavin, Lepping, Gjerloev, Farfield, et al., 2003; Slavin, Lepping, Gjerloev, Goldstein, et al., 2003; Nakamura et al., 2006; Chen et al., 2008; H. Wang, Lu, Huang, et al., 2016a). Generally, they are embedded within high-speed ion bulk flows and are believed to be produced by magnetic reconnection. The current density within the flux rope was explored previously, mainly based on the Curlometer technique (Dunlop et al., 2002; Slavin et al., 2003; Wang, Lu, Huang, et al., 2016a; Wang, Lu, Nakamura, Huang, Du, et al., 2016b). The results show that the current density is substantially enhanced within the flux rope and the current along its axis dominates in most situations, that is, the *y* direction at the magnetopause and in the magnetotail (Slavin et al., 2003; Wang, Lu, Huang, et al., 2016a; Wang, Lu, Nakamura, Huang, Du, et al., 2016b). Using the MMS measurements at the magnetopause, the current density was studied again and was found to be filamentary within the flux rope (Eastwood et al., 2016). In this paper, we further examine the current density within a series of three flux ropes observed at the magnetopause. For the first two flux ropes Fr1 and Fr2, well-separated filamentary currents j_y were observed; the widths of the filamentary currents and the gap between them were comparably sub ion scale, sometimes down to electron scale. By comparing the current density at the four satellites with a small separation (~10 km), we find that the current within the flux ropes was dynamic and could be still fragmenting. Regarding the Fr3, the current density was different from the other two ropes. In the Fr3, the current density j_y displayed a singular current layer with a few small peaks above the background value, except at mms2 where a thin filamentary current (300 ms) at 1103:08.2 UT was followed by a whole current layer (~1 s). One distinction that we can find between Fr3 and Fr1/Fr2 was the duration and thereby the size. The duration of Fr3 was about 6 s, while the other two flux ropes Fr1 and Fr2 were only about 1 s. So the size of the Fr3 was significantly larger than those of Fr1 and Fr2. However, it is still unclear how the size affects the current density within the rope. Another difference between Fr3 and Fr1/Fr2 was the distance between them to the expected X line. Since Fr3 was observed last inside the southern ion flows, it was closer to the X line than Fr1 and Fr2 (Figure 4). Thus, it is possible that Fr3 was created most newly and still kept the current feature when it was produced. If this speculation is true, the current density inside the flux rope should be singular when the rope is created and then fragmenting into a series of filamentary currents later. We further studied the flux transfer events between September and December 2015 during the first phase of MMS. In most situations, the current density inside the flux rope displays a series of filamentary currents as shown in the Fr1 and Fr2. The speculation for the evolution of the current density within the flux rope will be further investigated.

The ratio of the perpendicular to the parallel current density was calculated within the flux ropes and was used to recognize whether the flux rope was force-free or not. If the ratio was very small, it means that the parallel current was much stronger than the perpendicular current; that is, the magnetic field tends to be force-free. As for the flux ropes, Fr1 and Fr2, the magnetic field tended to be force-free in a narrow region near the centers, while at the flux rope Fr3, the magnetic field was nonforce free. It is unclear whether the state of the force-free is associated with the current appearance (filamentary currents or a singular current) within the flux rope.

Using the Cluster measurements in the magnetotail, Wang, Lu, Huang, et al. (2016a) found that the reconnection ion diffusion region is filled with magnetic flux ropes and these flux ropes interact with each other via magnetic reconnection, called coalescence. The key evidence for the coalescence includes the induced electric current layer between two neighboring flux ropes and the strong energy dissipation within the layer. The coalescence of flux ropes was also found to occur away from the reconnection site (Zhao, Wang, et al., 2016). However, the coalescence of magnetic flux ropes has not been observed at the magnetopause. Most recently, Øieroset et al. (2016) found a strong ion jet within one flux rope at the magnetopause. By comparing with simulation results, they concluded that the ion jet in fact was created by reconnection occurring within the flux ropes. Naturally, the authors suggested that the coalescence was one possible candidate for the reconnection process. However, only one flux ropes was identified in that event.

In this paper, we report a series of three flux ropes moving southward at the magnetopause. We investigated the interregions between Fr1 and Fr2, and between Fr2 and Fr3. In the interregion between Fr1 and Fr2, no reconnection signature was observed. Thus, there was no ongoing reconnection while the spacecraft crossed the interregion between the Fr1 and Fr2. As for the interregion between Fr2 and Fr3, the localized compression between the trailing edge of the Fr2 and the leading edge of the Fr3 was evident. The induced current layer was directed to the dawnside and its current was carried by electrons. The magnetic field intensity was asymmetric at both sides of this current layer. While the spacecraft crossed this asymmetric current layer, the Hall magnetic field and electric field were observed. The Hall magnetic field was asymmetric: the quadrant adjacent to the side of the weaker reconnecting field was wider than that at the other side, as shown in Figure 4. The Hall electric field pointing to the south was observed and the counterpart directed to the north was not found. The observed asymmetric distribution of the Hall magnetic field and the unipolar Hall electric field here are consistent with the previous observations at the magnetopause (Wang et al., 2017) and the prediction of numerical simulations (Hesse et al., 2016; Huang et al., 2014; Pritchett & Mozer, 2009; Shay et al., 2016). Furthermore, the expected reconnection electron outflows, comparable to the local Alfven speed, were bounded by the inflowing electrons, and the parallel electric field was detected in the separatrix region. Therefore, we conclude that a reconnection was occurring between the Fr2 and Fr3. In other words, the two flux ropes were interacting via magnetic reconnection.

In the coalescence events observed in the magnetotail, the compression between two flux ropes was always caused by the collision of one flux rope with the neighboring one ahead of it (Wang et al., 2016a; Zhao, Wang, et al., 2016). In the present event, however, Fr2 was moving southward and was faster than the Fr3, which was located north of Fr2 and was also moving southward. Therefore, it is impossible that there was any compression between them, if the structures of the two flux ropes did not change. B_x in the leading part (down to -12 nT) of the Fr3 was stronger than that (up to 7 nT) in its trailing part (Figure 2a). The most probable explanation is that the Fr3 was expanding along the z direction and the expanding speed was larger than the propagation speed of the Fr2. As a result, the leading edge of the Fr3 collided with the trailing part of the Fr2, and then reconnection was triggered between them. As stated above, reconnection was only found in the region between Fr2 and Fr3 while there was no reconnection signature between Fr1 and Fr2. Therefore, it seems that the temporal compression of the local magnetic field was one necessary condition for the trigger of the coalescence.

In conclusion, a series of three flux ropes were identified in the southern outflow of magnetic reconnection at the magnetopause. The current densities within the flux ropes and the interaction regions between the flux ropes were investigated in detail. The current density was found to be well-separated filamentary currents inside the first two flux ropes but displayed a singular current layer in the largest flux rope which was closest to the X line. The last two flux ropes were interacting via magnetic reconnection while no reconnection was occurring between the first two flux ropes. We suggested that the compression of the local magnetic field was one necessary condition for the occurrence of the coalescence between two neighboring flux ropes.

Acknowledgments
All the MMS data used in this work are available at the MMS data center (https://lasp.colorado.edu/mms/sdc/). This work is supported by the National Science Foundation of China (NSFC) grants (41674143, 41474126, 41331067, and 41421063) and by the National Basic Research Program of China (2013CBA01503). The work at Austria is supported by the Austrian Science Fund (FWF) I2016-N20.

References

Bhattacharjee, A., Huang, Y. M., Yang, H., & Rogers, B. (2009). Fast reconnection in high-Lundquist-number plasmas due to the plasmoid Instability. *Physics of Plasmas*, *16*(11). https://doi.org/10.1063/1.3264103

Burch, J. L., Moore, T. E., Torbert, R. B., & Giles, B. L. (2016). Magnetospheric Multiscale overview and science objectives. *Space Science Reviews*, *199*(1–4), 5–21. https://doi.org/10.1007/s11214-015-0164-9

Burch, J. L., Torbert, R. B., Phan, T. D., Chen, L. J., Moore, T. E., Ergun, R. E., … Gershman, D. J. (2016). Electron-scale measurements of magnetic reconnection in space. *Science*. https://doi.org/10.1126/science.aaf2939

Chen, L. J., Bhattacharjee, A., Puhl-Quinn, P. A., Yang, H., Bessho, N., Imada, S., … Georgescu, E. (2008). Observation of energetic electrons within magnetic islands. *Nature Physics*, *4*(1), 19–23. https://doi.org/10.1038/Nphys777

Daughton, W., Roytershteyn, V., Albright, B. J., Karimabadi, H., Yin, L., & Bowers, K. J. (2009). Transition from collisional to kinetic regimes in large-scale reconnection layers. *Physical Review Letters*, *103*(6), 065004. https://doi.org/10.1103/Physrevlett.103.065004

Daughton, W., Roytershteyn, V., Karimabadi, H., Yin, L., Albright, B. J., Bergen, B., & Bowers, K. J. (2011). Role of electron physics in the development of turbulent magnetic reconnection in collisionless plasmas. *Nature Physics*, *7*(7), 539–542. https://doi.org/10.1038/Nphys1965

Daughton, W., Scudder, J., & Karimabadi, H. (2006). Fully kinetic simulations of undriven magnetic reconnection with open boundary conditions. *Physics of Plasmas*, *13*(7). https://doi.org/10.1063/1.2218817

Drake, J. F., Swisdak, M., Che, H., & Shay, M. A. (2006). Electron acceleration from contracting magnetic islands during reconnection. *Nature*, *443*(7111), 553–556. https://doi.org/10.1038/Nature05116

Dungey, J. W. (1961). Interplanetary magnetic field and auroral zones. *Physical Review Letters*, *6*(2), 47. https://doi.org/10.1103/PhysRevLett.6.47

Dunlop, M. W., Balogh, A., Glassmeier, K. H., & Robert, P. (2002). Four-point Cluster application of magnetic field analysis tools: The Curlometer. *Journal of Geophysical Research*, *107*(A11), 1384. https://doi.org/10.1029/2001JA005088

Dunlop, M. W., Taylor, M. G. G. T., Davies, J. A., Owen, C. J., Pitout, F., Fazakerley, A. N., … Sonnerup, B. (2005). Coordinated Cluster/Double Star observations of dayside reconnection signatures. *Annales de Geophysique*, *23*(8), 2867–2875.

Eastwood, J. P., Phan, T. D., Cassak, P. A., Gershman, D. J., Haggerty, C., Malakit, K., … Wang, S. (2016). Ion-scale secondary flux ropes generated by magnetopause reconnection as resolved by MMS. *Geophysical Research Letters*, *43*, 4716–4724. https://doi.org/10.1002/2016GL068747

Eastwood, J. P., Phan, T. D., Fear, R. C., Sibeck, D. G., Angelopoulos, V., Øieroset, M., & Shay, M. A. (2012). Survival of flux transfer event (FTE) flux ropes far along the tail magnetopause. *Journal of Geophysical Research*, *117*, A08222. https://doi.org/10.1029/2012JA017722

Ergun, R. E., Andersson, L., Tao, J., Angelopoulos, V., Bonnell, J., McFadden, J. P., … Baumjohann, W. (2009). Observations of double layers in Earth's plasma sheet. *Physical Review Letters*, *102*, 155002. https://doi.org/10.1103/PhysRevLett.102.155002

Ergun, R. E., Tucker, S., Westfall, J., Goodrich, K. A., Malaspina, D. M., Summers, D., … Cully, C. M. (2016). The axial double probe and fields signal processing for the MMS mission. *Space Science Reviews*, *199*(1–4), 167–188. https://doi.org/10.1007/s11214-014-0115-x

Farrugia, C. J., Torbert, R. B., Southwood, D. J., Cowley, S. W., Vrublevskis, A., Vaivads, A., … Smith, C. W. (2011). "Crater" flux transfer events: Highroad to the X line? *Journal of Geophysical Research*, *116*, A02204. https://doi.org/10.1029/2010JA015495

Fear, R. C., Milan, S. E., Fazakerley, A. N., Lucek, E. A., Cowley, S. W. H., & Dandouras, I. (2008). The azimuthal extent of three flux transfer events. *Annales de Geophysique*, *26*(8), 2353–2369.

Fu, X. R., Lu, Q. M., & Wang, S. (2006). The process of electron acceleration during collisionless magnetic reconnection. *Physics of Plasmas*, *13*, 012309.

Hasegawa, H., Wang, J., Dunlop, M. W., Pu, Z. Y., Zhang, Q. H., Lavraud, B., … Bogdanova, Y. V. (2010). Evidence for a flux transfer event generated by multiple X-line reconnection at the magnetopause. *Geophysical Research Letters*, *37*, L16101. https://doi.org/10.1029/2010GL044219

Hesse, M., Liu, Y. H., Chen, L. J., Bessho, N., Kuznetsova, M., Birn, J., & Burch, J. (2016). On the electron diffusion region in asymmetric reconnection with a guide magnetic field. *Geophysical Research Letters*, *43*, 2359–2364. https://doi.org/10.1002/2016GL068373

Hesse, M., & Schindler, K. (1988). A theoretical foundation of general magnetic reconnection. *Journal of Geophysical Research*, *93*(A6), 5559–5567. https://doi.org/10.1029/JA093iA06p05559

Huang, C., Lu, Q. M., Lu, S., Wang, P. R., & Wang, S. (2014). The effect of a guide field on the structures of magnetic islands formed during multiple X line reconnections: Two-dimensional particle-in-cell simulations. *Journal of Geophysical Research*, *119*, 798–807. https://doi.org/10.1002/2013JA019249

Huang, C., Lu, Q., Guo, F., Wu, M. Y., Du, A. M., & Wang, S. (2015). Magnetic islands formed due to the Kelvin-Helmholtz instability in the outflow region of collisionless magnetic reconnection. *Geophysical Research Letters*, *42*, 7282–7286. https://doi.org/10.1002/2015GL065690

Hwang, K. J., Sibeck, D. G., Giles, B. L., Pollock, C. J., Gershman, D., Avanov, L., … Burch, J. L. (2016). The substructure of a flux transfer event observed by the MMS spacecraft. *Geophysical Research Letters*, *43*(18), 9434–9443. https://doi.org/10.1002/2016GL070934

Koga, D., Gonzalez, W. D., Mozer, F. S., Silveira, M. V. D., & Cardoso, F. R. (2014). Larmor electric field observed at the Earth's magnetopause by Polar satellite. *Physics of Plasmas*, *21*(10), 100701. https://doi.org/10.1063/1.4897935

Lee, L. C., & Fu, Z. F. (1985). A theory of magnetic-flux transfer at the Earth's magnetopause. *Geophysical Research Letters*, *12*(2), 105–108. https://doi.org/10.1029/GL012i002p00105

Lindqvist, P. A., Olsson, G., Torbert, R. B., King, B., Granoff, M., Rau, D., … Tucker, S. (2016). The spin-plane double probe electric field instrument for MMS. *Space Science Reviews*, *199*(1–4), 137–165. https://doi.org/10.1007/s11214-014-0116-9

Loureiro, N. F., Schekochihin, A. A., & Cowley, S. C. (2007). Instability of current sheets and formation of plasmoid chains. *Physics of Plasmas*, *14*(10), 100703. https://doi.org/10.1063/1.2783986

Lu, S., Lu, Q., Huang, C., & Wang, S. (2013). The transfer between electron bulk kinetic energy and thermal energy in collisionless magnetic reconnection. *Physics of Plasmas*, *20*, 061203

Malakit, K., Shay, M. A., Cassak, P. A., & Ruffolo, D. (2013). New electric field in asymmetric magnetic reconnection. *Physical Review Letters*, *111*(13), 135001. https://doi.org/10.1103/PhysRevLett.111.135001

Moldwin, M. B., & Hughes, W. J. (1991). Plasmoids as magnetic-flux ropes. *Journal of Geophysical Research*, *96*(A8), 14,051–14,064. https://doi.org/10.1029/91JA01167

Nakamura, R., Baumjohann, W., Asano, Y., Runov, A., Balogh, A., Owen, C. J., … Reme, H. (2006). Dynamics of thin current sheets associated with magnetotail reconnection. *Journal of Geophysical Research*, *111*, A11206. https://doi.org/10.1029/2006JA011706

Newman, D. L., Goldman, M. V., Ergun, R. E., & Mangeney, A. (2001). Formation of double layers and electron holes in a current-driven space plasma. *Physical Review Letters*, *87*. https://doi.org/10.1103/PhysRevLett.87.255001

Øieroset, M., Phan, T. D., Eastwood, J. P., Fujimoto, M., Daughton, W., Shay, M. A., … Glassmeier, K. H. (2011). Direct evidence for a three-dimensional magnetic flux rope flanked by two active magnetic reconnection X lines at Earth's magnetopause. *Physical Review Letters*, *107*(16), 165007. https://doi.org/10.1103/PhysRevLett.107.165007

Øieroset, M., Phan, T. D., Haggerty, C., Shay, M., & Eastwood, J. (2016). MMS observations of large guide field symmetric reconnection between colliding reconnection jets at the center of a magnetic flux rope at the magnetopause. *Geophysical Research Letters*, *43*, 5536–5544. https://doi.org/10.1002/2016GL069166

Oka, M., Phan, T. D., Krucker, S., Fujimoto, M., & Shinohara, I. (2010). Electron acceleration by multi-island coalescence. *The Astrophysical Journal*, *714*(1), 915–926. https://doi.org/10.1088/0004-637x/714/1/915

Owen, C. J., Fazakerley, A. N., Carter, P. J., Coates, A. J., Krauklis, I. C., Szita, S., … Dunlop, M. W. (2001). Cluster PEACE observations of electrons during magnetospheric flux transfer events. *Annales de Geophysique*, *19*(10–12), 1509–1522.

Pollock, C., Moore, T., Jacques, A., Burch, J., Gliese, U., Saito, Y., … Zeuch, M. (2016). Fast plasma investigation for Magnetospheric Multiscale. *Space Science Reviews*, *199*(1–4), 331–406. https://doi.org/10.1007/s11214-016-0245-4

Pritchett, P. L., & Mozer, F. S. (2009). Asymmetric magnetic reconnection in the presence of a guide field. *Journal of Geophysical Research*, *114*, A11210. https://doi.org/10.1029/2009JA014343

Pu, Z. Y., Raeder, J., Zhong, J., Bogdanova, Y. V., Dunlop, M., Xiao, C. J., … Fazakerley, A. (2013). Magnetic topologies of an in vivo FTE observed by Double Star/TC-1 at Earth's magnetopause. *Geophysical Research Letters*, *40*, 3502–3506. https://doi.org/10.1002/grl.50714

Raeder, J. (2006). Flux transfer events: 1. Generation mechanism for strong southward IMF. *Annales de Geophysique*, *24*(1), 381–392.
Russell, C. T., & Elphic, R. C. (1978). Isee-1 and Isee-2 observations of flux-transfer events on dayside magnetopause. *Eos. Transactions American Geophysical*, *59*(12), 1162–1162.
Russell, C. T., Anderson, B. J., Baumjohann, W., Bromund, K. R., Dearborn, D., Fischer, D., … Richter, I. (2016). The Magnetospheric Multiscale magnetometers. *Space Science Reviews*, *199*(1–4), 189–256. https://doi.org/10.1007/s11214-014-0057-3
Samtaney, R., Loureiro, N. F., Uzdensky, D. A., Schekochihin, A. A., & Cowley, S. C. (2009). Formation of plasmoid chains in magnetic reconnection. *Physical Review Letters*, *103*(10), 105004. https://doi.org/10.1103/Physrevlett.103.105004
Scholer, M. (1988). Magnetic-flux transfer at the magnetopause based on single X-line bursty reconnection. *Geophysical Research Letters*, *15*(4), 291–294. https://doi.org/10.1029/GL015i004p00291
Schwartz, S. J. (1998). Shock and discontinuity normals, mach numbers and related parameters. In G. Paschmann, & P. W. Daly (Eds.), *Analysis methods for multi-spacecraft data* (pp. 249–270), Bern: International Space Science Institute.
Shay, M., Phan, T., Haggerty, C. C., Fujimoto, M., Drake, J. F., Malakit, K., … Swisdak, M. (2016). Kinetic signatures of the region surrounding the X line in asymmetric (magnetopause) reconnection. *Geophysical Research Letters*, *43*, 4145–4154. https://doi.org/10.1002/2016GL069034
Sibeck, D. G., Siscoe, G. L., Slavin, J. A., Smith, E. J., Bame, S. J., & Scarf, F. L. (1984). Magnetotail flux ropes. *Geophysical Research Letters*, *11*, 1090–1093. https://doi.org/10.1029/GL011i010p01090
Slavin, J. A., Lepping, R. P., Gjerloev, J., Fairfield, D. H., Hesse, M., Owen, C. J., … Mukai, T. (2003). Geotail observations of magnetic flux ropes in the plasma sheet. *Journal of Geophysical Research*, *108*(A1), 1015. https://doi.org/10.1029/2002JA009557.
Slavin, J. A., Lepping, R. P., Gjerloev, J., Goldstein, M. L., Fairfield, D. H., Acuna, M. H., …, Bosqued, J. M. (2003). Cluster electric current density measurements within a magnetic flux rope in the plasma sheet. *Geophysical Research Letters*, *30*(7), 1362. https://doi.org/10.1029/2002GL016411.
Sonnerup, B. U. O., & Cahill, L. J. Jr. (1968). Explorer 12 observations of the magnetopause current layer. *Journal of Geophysical Research*, *73*, 1757–1770. https://doi.org/10.1029/JA073i005p01757
Southwood, D. J., Farrugia, C. J., & Saunders, M. A. (1988). What are flux-transfer events. *Planetary and Space Science*, *36*(5), 503–508. https://doi.org/10.1016/0032-0633(88)90109-2
Teh, W. L., Nakamura, T. K. M., Nakamura, R., Baumjohann, W., Russell, C. T., Pollock, C., … Giles, B. L. (2017). Evolution of a typical ion-scale magnetic flux rope caused by thermal pressure enhancement. *Journal of Geophysical Research*, *122*, 2040–2050. https://doi.org/10.1002/2016JA023777
Varsani, A., Owen, C. J., Fazakerley, A. N., Forsyth, C., Walsh, A. P., Andre, M., … Carr, C. M. (2014). Cluster observations of the substructure of a flux transfer event: Analysis of high-time-resolution particle data. *Annales de Geophysique*, *32*(9), 1093–1117. https://doi.org/10.5194/angeo-32-1093-2014
Wang, H. Y., Lu, Q., Huang, C., & Wang, S. (2016a). The mechanisms of electron acceleration during multiple X line magnetic reconnection with a guide field. *The Astrophysical Journal*, *821*(84).
Wang, R. S., Lu, Q., Khotyaintsev, Y. V., Volwerk, M., Du, A., Nakamura, R., … Wu, M. (2014). Observation of double layer in the separatrix region during magnetic reconnection. *Geophysical Research Letters*, *41*, 4851–4858. https://doi.org/10.1002/2014GL061157
Wang, R. S., Lu, Q. M., Nakamura, R., Huang, C., Du, A. M., Guo, F., … Wang, S. (2016a). Coalescence of magnetic flux ropes in the ion diffusion region of magnetic reconnection. *Nature Physics*, *12*(3), 263–267. https://doi.org/10.1038/Nphys3578
Wang, R. S., Lu, Q. M., Nakamura, R., Huang, C., Li, X., Wu, M. Y., … Wang, S. (2016b). Electrostatic and electromagnetic fluctuations detected inside magnetic flux ropes during magnetic reconnection. *Journal of Geophysical Research*, *121*, 9473–9482. https://doi.org/10.1002/2016JA022906
Wang, R. S., Nakmura, R., Lu, Q. M., Baumjohann, W., Ergun, R. E., Burch, J. L., … Wang, S. (2017). Electron-scale quadrants of the Hall magnetic field observed by the Magnetospheric Multiscale spacecraft during asymmetric reconnection. *Physical Review Letters*, *118*, 175101.
Xiao, C. J., Pu, Z. Y., Ma, Z. W., Fu, S. Y., Huang, Z. Y., & Zong, Q. G. (2004). Inferring of flux rope orientation with the minimum variance analysis technique. *Journal of Geophysical Research*, *109*, A11218. https://doi.org/10.1029/2004JA010594
Zenitani, S., Shinohara, I., & Nagai, T. (2012). Evidence for the dissipation region in magnetotail reconnection. *Geophysical Research Letters*, *39*, L11102. https://doi.org/10.1029/2012GL051938
Zhang, H., Kivelson, M. G., Angelopoulos, V., Khurana, K. K., Pu, Z. Y., Walker, R. J., … Phan, T. (2012). Generation and properties of in vivo flux transfer events. *Journal of Geophysical Research*, *117*, A05224. https://doi.org/10.1029/2011JA017166
Zhao, C., Russell, C. T., Strangeway, R. J., Petrinec, S. M., Paterson, W. R., Zhou, M., … Wei, H. Y. (2016). Force balance at the magnetopause determined with MMS: Application to flux transfer events. *Geophysical Research Letters*, *43*, 11,941–11,947. https://doi.org/10.1002/2016GL071568
Zhao, Y., Wang, R., Lu, Q. M., Du, A. M., Yao, Z. H., & Wu, M. Y. (2016). Coalescence of magnetic flux ropes observed in the tailward high-speed flows. *Journal of Geophysical Research*, *121*, 10,898–10,909. https://doi.org/10.1002/2016JA023526
Zhong, J., Pu, Z. Y., Dunlop, M. W., Bogdanova, Y. V., Wang, X. G., Xiao, C. J., … Eastwood, J. P. (2013). Three-dimensional magnetic flux rope structure formed by multiple sequential X-line reconnection at the magnetopause. *Journal of Geophysical Research*, *118*, 1904–1911. https://doi.org/10.1002/jgra.50281
Zong, Q.-G., Wilken, B., Reeves, G. D., Daglis, I. A., Doke, T., Iyemori, T., … Yamamoto, T. (1997). Geotail observation of energetic ion species and magnetic field in plasmoid-like structure in the course of an isolated substorm event. *Journal of Geophysical Research*, *103*, 11,409–11,428. https://doi.org/10.1029/97JA00076